

Particle-Electrode Impacts: Evidencing Partial Versus Complete Oxidation via Variable Temperature Studies

Christopher A. Little, Xiuting Li, Christopher Batchelor-McAuley, Neil P. Young and Richard G. Compton*

* corresponding author: Richard G. Compton, Department of Chemistry, Physical & Theoretical Chemistry Laboratory, University of Oxford, South Parks Road, Oxford, OX1 3QZ, United Kingdom

Email: richard.compton@chem.ox.ac.uk. Tel: +44(0)1865275 957 Fax: +44(0)1865275410

Abstract

The partial electro-oxidation of large silver nanoparticles is evidenced by comparing the charges passed in nanoparticle-electrode impacts at a range of temperatures. For larger silver nanoparticles (>100 nm diameter), the variation in the charge passed per nano-impact event at higher temperatures demonstrates that single nanoparticles undergo multiple oxidations events at the electrode, and these oxidations do not go to completion. In contrast, the relative insensitivity of the charge passed in the electrode impacts of smaller silver nanoparticles (<50 nm diameter) to the variation of temperature is consistent with their complete oxidation.

Keywords

Silver nanoparticles, partial oxidation, variable temperature, nano-impacts

Introduction

The dynamics of a particle differ markedly when it is situated near or at an interface. This interaction between the particle and a surface is influenced by a range of chemical and physical phenomena. First, when close to a boundary wall a particle's hydrodynamic mobility is decreased leading to its diffusion being 'hindered' [1,2]. Furthermore, at very short distances the structure of the solvent leads to an oscillatory force varying on the length scale of the solvent [3]. Second, many surfaces when submerged in an aqueous solution have an associated surface charge; this charge may lead to electrostatic interactions – repulsive or attractive – of the particle with the interface [4]. Third, chemical binding, including hydrogen bonding, of the particle to the surface can significantly influence its behaviour [5,6]. Fourth, van der Waals forces between the surface and the particle are ever present and predominantly lead to an attractive interaction between the particle and surface [4,7]. These interactions can become even more complex when considering the dynamics of agglomeration near surfaces, where long range attractive forces between particles may arise during the course of such many-body interactions [8]. The particle-surface interaction dynamics will be sensitive to the local temperature. Moreover, apart from being of fundamental interest, these particle-surface interactions are important for a range of both biological and technological processes.

The area of single particle detection has expanded significantly over the previous decade [9,10], here an electrode is submerged into a solution containing nanoparticles and upon random collision with an electrified interface, a reaction of or at the nanoparticle can be induced to occur. The rate of this reaction is extremely sensitive to the particle-surface separation distance. Assuming the electrons are transferred between the electrode and the nanoparticle by tunnelling and that this transfer is the rate determining step for the reaction then the resulting current will be proportional to $e^{-\beta r}$ [11,12], for water the magnitude of β is $\sim 1.6 \text{ \AA}^{-1}$ [13], where r is the tunnelling distance. In a destructive nano-impact [14], a redox active nanoparticle is used and the direct oxidation or reduction of the individual particle is driven by the applied electrode potential. In the case of silver nanoparticle (AgNP) oxidation and for small particles of ca. 20 nm diameter, in most experimental cases the oxidation of the particle likely goes to completion and the resulting shape of the spike in current commonly predominantly reflects the bandwidth of the used measurement electronics [15]. However, as first experimentally demonstrated in 2015, for larger particles (ca. 100 nm diameter) the individual nano-reactions do not necessarily lead to complete oxidation of the particle without the presence of high concentrations of electrolyte, particularly in the presence of

chloride [16]. In more recent work in the literature this was demonstrated to be, as theoretically predicted in 2012 [17], likely due to the nano-motion of the particle adjacent to the interface such that for larger particles there is an increased probability of material being 'lost' from the interface prior to the reaction going to completion [18,19]. The shape and magnitude of the individual spike maxima are found to be experimentally sensitive to both the electrolyte concentration and the applied electrode potential [20,21]. The charge passed during a single nano-impact event gives a *direct* measure of the amount of material oxidised during the course of a single event. However, challengingly, unambiguously determining if such an oxidation event corresponds to a complete or partial oxidation (or reduction) of a nanoparticle can presently only be evidenced by comparison, on a statistical basis, of the experimental electrochemical data with other sizing information such as that obtained from electron microscopy. This issue is further compounded by the fact that in order for a quantitative comparison to be made between the different techniques a number of important factors, including the nanoparticle population's morphology, the measurement electronics' signal-to-noise ratio and the influence of the particle's diffusion coefficient have to be fully accounted for [22]. If a single nanoparticle event does not go to completion then, assuming that the extent to which the reaction proceeds is determined by a balance of kinetic factors, such as the dynamic movement of the particle adjacent to the interface and the electrochemical oxidation kinetics, the charge passed per event will be anticipated to be temperature sensitive.

This work evidences the partial oxidation of large (~100 nm diameter) silver nanoparticles using a variable temperature nano-impacts study and subsequent comparison of this data with TEM imaging. The study yields insights into the processes occurring during the nanoparticle oxidation reaction. An analogous study is carried out on smaller 50 nm silver nanoparticles to demonstrate the value of varying the temperature in establishing the extent of oxidation of nanoparticles.

Experimental

Chemical Reagents

Spherical citrate-AgNPs of ca. 50 nm and 100 nm (Nanoxact, 0.02 mg mL⁻¹ silver, 2 mM sodium citrate) were purchased from Nanocomposix, USA. Potassium Chloride ($\geq 99.0\%$) was obtained from Sigma-Aldrich and was used as received without further purification. Solutions were prepared using deionized water (Millipore) with a resistivity of no less than 18.2 M Ω cm at 25°C.

Nanoparticle Characterisation

UV-Vis studies were carried out using a Shimadzu UV-1800 spectrophotometer in disposable cuvettes (Eppendorf UVette, Sigma-Aldrich) using a 10 mm optical path length at wavelengths of $\lambda = 300\text{--}1100$ nm for the 100 nm AgNPs and $\lambda = 300\text{--}700$ nm for the 50 nm AgNPs.

Transmission electron microscopy (TEM) imaging of the 50 nm and 100 nm AgNPs was carried out using a JEOL JEM-3000F instrument with an accelerating voltage of 300 kV. The samples were prepared by drop-casting suspensions of 48 pM 50 nm AgNPs in 2 mM sodium citrate or 6 pM 100 nm AgNPs in 2 mM sodium citrate onto carbon grids (Agar Scientific Ltd, UK) and allowing them to dry. Subsequent image extraction and analysis was performed using ImageJ software.

Nano-impacts

Nano-impact experiments were carried out using a home-built low noise potentiostat, as described previously [23]. The signal was processed by filtering digitally (4-pole Bessel) to 100 Hz using a script written in Python 3.5. Measurements were carried out at a carbon microdisc ($d = 33\text{ }\mu\text{m}$, IJ Cambria Scientific Ltd, U.K.) working electrode. A saturated calomel electrode (BASi, USA) was used as a reference electrode, and a platinum wire was used as a counter electrode. Cyclic voltammetric measurements were carried out on 12 pM suspensions of 50 nm and 1.5 pM suspensions of 100 nm AgNPs containing 20 mM KCl, initially scanning anodically in the potential range of 0.0 V to 0.8 V (vs. SCE) at a scan rate of 10 mV s⁻¹. A 16-bit DAC was used to provide the waveform with a full potentiostat range of ± 2 V, effectively corresponding to staircase voltammetry with a step size of 61 μV . Chronoamperometry was performed on the same solutions, with the potential stepped to 0.426 V (vs. SCE) for 60 s. These chronoamperometric measurements were repeated with varying immersion times of 10, 30, 90, 120 and 240 s for both nanoparticle sizes. Prior to each experiment, the working electrode was polished on aqueous slurries of 1.0, 0.3 and 0.05 μm alumina in descending order of size, before rinsing with deionized water. Nano-impact spikes were identified and

analysed using a script written in Python 3.5. The details of the signal analysis have been described elsewhere [22]. These studies were carried out at 15°C, 25°C and 50°C for both sizes of nanoparticles, and additionally 35°C for the 100 nm nanoparticles. The thermostating system used in the variable temperature study was fabricated in-house as described elsewhere [21], and has been optimised to minimise the effects of natural convection. It is noted that natural convection can never be completely eliminated; however, its effects are lessened in interfacial experiments such as those studied in this work compared to techniques such as SECM where they can be prohibitive [24]. Here, the effects of natural convection are mitigated not only by the proximity of the nanoparticles to the boundary, but also to their significantly lower diffusion coefficients compared to molecular species.

Results and Discussion

This work begins with the characterisation of the two sizes of nanoparticles by use of UV-Vis spectroscopy and TEM imaging. Next, artefacts of the electrochemical analysis are accounted for using chronoamperometry. Finally, cyclic voltammetry is employed as a function of temperature to explore the partial oxidation of the larger nanoparticles, and to confirm the complete oxidation of the smaller nanoparticles.

Nanoparticle Characterisation

First, the stabilities of the 50 nm and 100 nm AgNPs suspensions were investigated by means of UV-Vis spectroscopy in varying electrolytes at both 25°C and 50°C. AgNPs are strongly plasmonic [25], exhibiting a strong peak in the visible region at *ca.* 400 nm, a wavelength that is dependent on NP size, shape, environment and NP potential [26]. Here, the magnitude of the peak of maximum absorbance will be used to assess their stabilities. Suspensions of 1.5 pM 100 nm AgNPs were prepared in deionised water, with 20 mM KCl or 20 mM KCl + 1.5 mM citrate. Figure 1 a) presents the UV-Vis spectrum for the suspension in 20 mM KCl at 25°C. The two peaks at *ca.* 495 nm and 410 nm reflect the dipolar and quadrupolar resonance modes observed for larger nanoparticles [27]. The inlay of Figure 1 a) depicts the relative absorbance at 495 nm as a function of time and electrolyte. It can be seen that the 100 nm AgNPs are extremely stable over a 40 minute period in deionised water (noting the 0.5 mM citrate present from the AgNP stock solution), with the absorbance only dropping 1% at 25°C and 4% at 50°C. As the ionic strength increases, the stability falls; the presence of 20 mM KCl causes a 45% and 61% decrease in peak absorbance at 25°C and 50°C respectively, whilst the presence

of 20 mM KCl and an extra 1.5 mM citrate (total 2 mM citrate, including that present from the stock solution) leads to a decrease of 53% and 66%. The decrease in stability with increasing ionic strength can be rationalised on the basis of the DLVO theory of colloidal stability; aggregation is induced by the screening of the nanoparticle surface charge [28,29]. Notably, the stark increase in the absorbance feature at wavelengths greater than ca. 700 nm over the 40 minutes is indicative of the agglomeration of the nanoparticles with time [30]. This nanoparticle agglomeration has previously been shown to be reversible [31]. To confirm this reversibility, the suspension of 100 nm AgNPs in 20 mM KCl and 1.5 mM citrate following the 40 minute period was sonicated for 10 minutes. This returned the peak absorbance to within 20% of its initial value; this data is presented in the SI section S1. Moreover, agitating the suspensions by means of bubbling N₂ gas through them for 1 minute was found to inhibit this agglomeration. The slightly lower stability of the 100 nm AgNPs at 50°C may be attributed to the higher thermal energy of the nanoparticles. Figure 1 b) depicts the equivalent UV-Vis spectra for a suspension of 12 pM 50 nm AgNPs in 20 mM KCl. From the inlay, the suspensions of 50 nm AgNPs were found to be more stable than the 100 nm AgNPs upon addition of electrolyte, with the peak absorbance at 426 nm in KCl remaining within 27% and 20 % of its initial value at 25°C and 50°C respectively after 40 minutes.

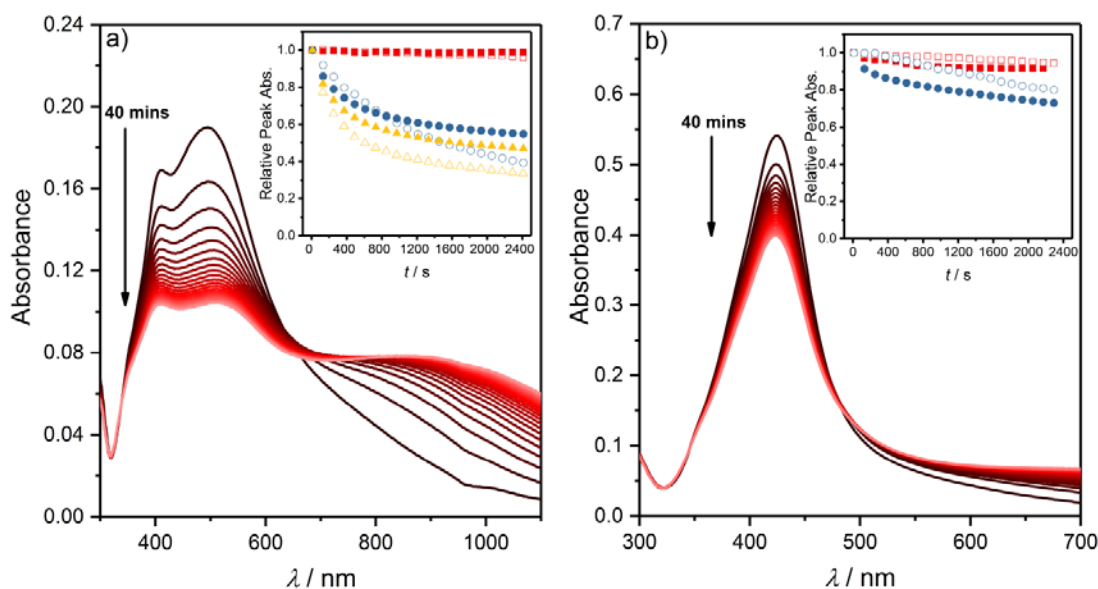


Figure 1. UV-Vis absorbance spectra of a 20 mM KCl solution at 25°C over a 40 minute period at 2 minute intervals containing a) 100 nm 1.5 pM AgNPs and b) 50 nm 12 pM AgNPs. The a) and b) inlays show the relative peak absorbance with time of the plasmonic peak at ca. 495 nm for a) and ca. 425 nm for b) in deionised water (red squares), 20 mM KCl (blue circles) and 20 mM KCl + 1.5 mM Citrate (yellow triangles). The filled points portray the data recorded at 25°C and the open points the data recorded at 50°C.

Whilst a degree of agglomeration occurs over this time period, the nanoparticles are metastable; this agglomeration is inhibited by agitation with N₂ bubbling. Given the use of 20 mM KCl as supporting electrolyte and the bubbling of solutions with N₂ between experiments, it is reasonable to conclude that the AgNPs suspensions are sufficiently stable over the time period (~30 minutes) of the subsequent electrochemical studies.

Next, the size distributions of the two batches of AgNPs were characterised by Transmission Electron Microscopy (TEM). To be able to directly compare the subsequent electrochemical studies to this data, the 2D projections imaged using TEM were converted into volume distributions and then presented as charge distributions *via* use of Faraday's first law, as described elsewhere [32]. Assumptions regarding the particle geometry are mandatory to obtain a volume distribution from the 2D representations of the particles; as can be seen in Figure 2, the nanoparticle population exhibits significant heterogeneity in their morphology. This necessitates the use of a correction factor (f) to account for the non-sphericity of the particles. The estimated nanoparticle volumes allow the charge to be calculated where the volume of the nanoparticle is equal to $\frac{4\pi R_s^3}{3} \times f$; R_s is the radius of sphere circumscribing the nanoparticle, and is taken to be the maximal radius for non-spherical particles (56% of the 50 nm batch and 70% of the 100 nm batch). The value of f is taken to be 1 for spherical particles (i.e. those appearing circular as a 2D projection) and for non-spherical particles to be 0.5, as used in previous work [32]. Figure 2 a) presents the cumulative frequency charge distributions plotted on a log scale, with representative images of 50 nm AgNPs b) and 100 nm AgNPs c). $N = 45$ and 81 for the two distributions respectively.

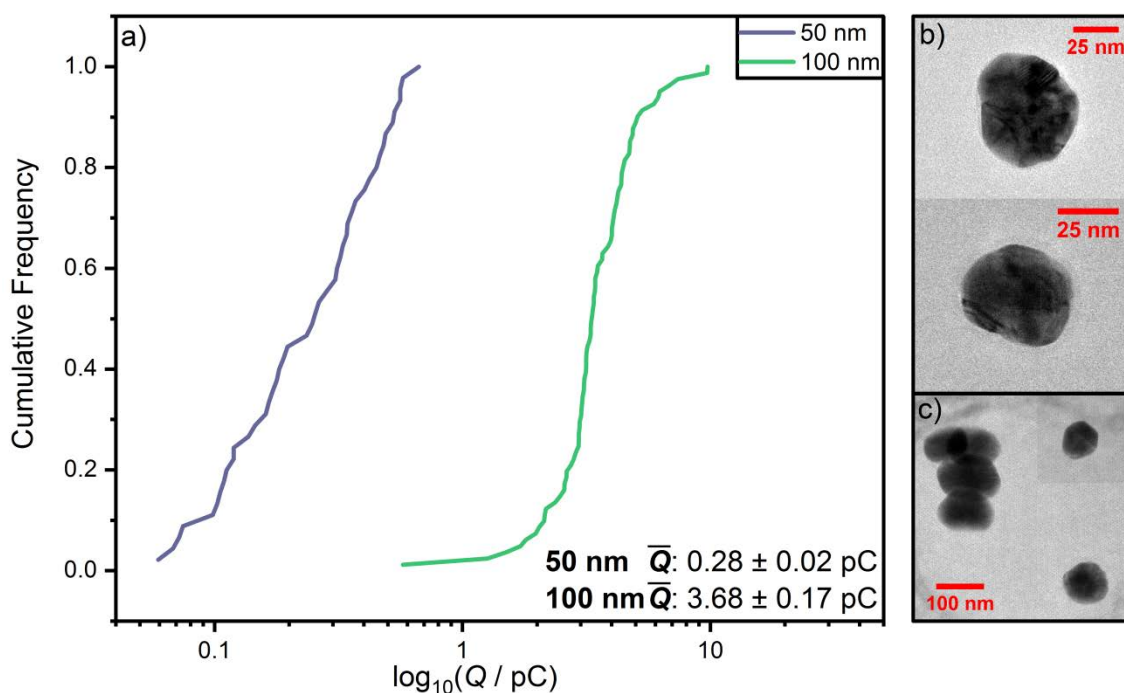


Figure 2. a) Cumulative frequency equivalent charge distribution calculated from TEM sizing of 50 nm and 100 nm AgNPs presented as solid purple and green lines respectively, taking into account correction factors for the non-sphericity of the particles. b) and c) show representative TEM images of 50 nm and 100 nm AgNPs respectively.

Nano-Impacts Study: Chronoamperometry

A series of chronoamperograms were run on solutions containing 12 pM 50 nm AgNPs or 1.5 pM 100 nm AgNPs and 20 mM KCl at a carbon microdisc electrode (33 μ m diameter) with the potential fixed at 0.426 V (vs. SCE) for 60 s. When AgNPs were present in solution, multiple oxidative current transients were observed in the current-time trace, representative examples are presented in the SI section S2. These current ‘spikes’ are well-documented as relating to the arrival and subsequent oxidation of the AgNPs at the electrochemical interface [14]. The time that the electrode was immersed in solution prior to the commencement of the chronoamperogram was varied from 10 s to 240 s. The cumulative number of spikes with time were identified and compared to the number theoretically predicted by assuming a steady-state flux to the electrode [33]:

$$(2) \quad J(t \rightarrow \infty) = 4DCr_e$$

The diffusion coefficient, D , has here been calculated *via* the Stokes-Einstein equation, assuming nanoparticle radii of 25 and 50 nm respectively. By using this equation to estimate the expected frequency of events it is implicitly assumed that the number of observed ‘spike’

events is controlled by the diffusive flux of the particles to the interface and that each nanoparticle is oxidised over the course of a single nano-event.

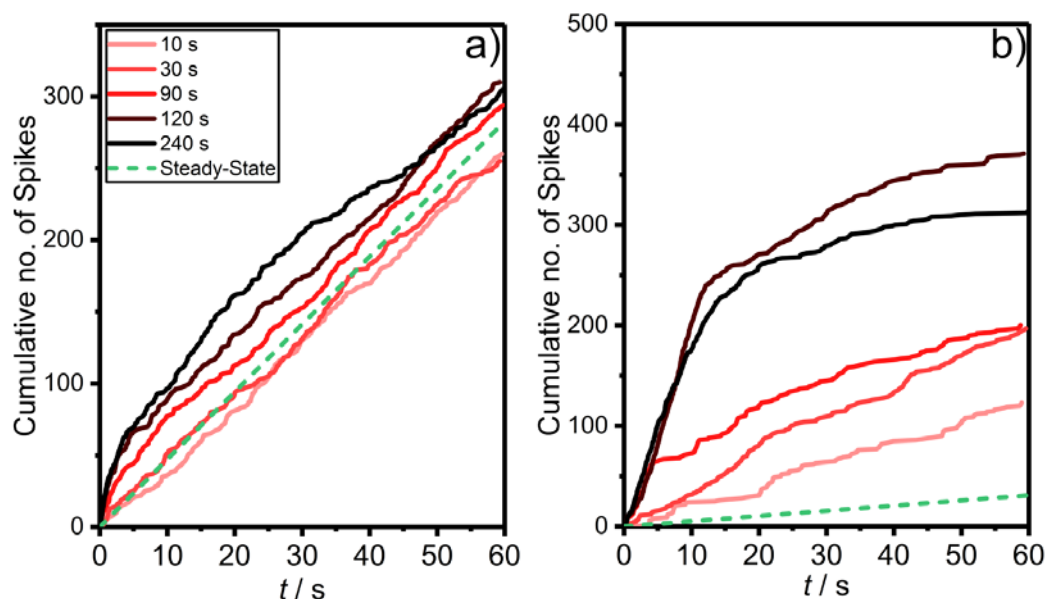


Figure 3. Cumulative number of spikes as a function of time for a series of chronoamperograms with varied immersion times for a) 50 nm AgNPs and b) 100 nm AgNPs. The different shades of solid red line show the immersion time of the electrode in solution prior to chronoamperogram commencement. The dashed green line depicts the predicted cumulative number of spikes based on a steady state flux to the electrode.

The data for the 50 nm AgNPs is presented in Figure 3 a); the measured frequency of nano-events is very closely comparable to that estimated on the basis of a steady-state flux to the electrode, and the frequency only indicates a very minimal sensitivity to how long the electrode has been pre-exposed to the nanoparticle solution. This data is consistent with the 50 nm particles being oxidised during the course of a single event. In the data there is a slightly increased frequency of spikes in the first 4 s before the cumulative number of spikes tends towards the predicted steady-state value at longer times. This small initial effect may reflect non-simultaneous oxidation of the material adsorbed onto the electrode surface.

The data for the analogous study on the 100 nm AgNPs is presented in Figure 3 b); for long immersion times, a large number of extremely small ($< \sim 0.2$ pC) spikes are prevalent early in the chronoamperogram ($t < 10$ s). Examples of such chronoamperograms with immersion times of 10 s and 240 s are presented in the SI section S3. Again, comparing the cumulative number of spikes observed with time to that predicted from a steady-state flux to the electrode is insightful. First, the initial gradients of the lines increase with the time the electrode has been immersed in the solution and hence exposed to the nanoparticle

suspension. This sensitivity to the period of exposure of the electrode to the nanoparticle suspension directly evidences the nanoparticles to be pre-concentrating at or near the electrochemical interface prior to the electrochemical experiment. It has previously been shown that AgNPs irreversibly adsorb to the electrode surface in the absence of potentiostatic control [34], a process likely reflected here. Moreover, studies have also demonstrated the adsorption of AgNPs to glass surfaces [32]; here the microdisc working electrode is encased in a glass sheath and hence it is reasonable to infer that the AgNPs may be adhering to both surfaces. This pre-concentration of particles in the vicinity leads to an increased probability of an electrochemical event occurring in the initial ca. 15 seconds of the electrochemical experiment. Second, it can be seen that even for short accumulation times, the gradients of the lines in Figure 3 b) are larger than the expected flux as calculated for the diffusive flux of the material to the electrode surface. This is in spite of several factors including particle-surface adsorption, agglomeration, or chemical kinetic processes that can lead to the observed impact frequency being less than one would predict using such a model [20,35]. Given the bespoke thermostating system used [21], over this experimental timescale it is unlikely that convective forces will enhance the flux of material to the interface. Consequently, this increased rate of the nano-events evidences that each nanoparticle is likely undergoing only partial oxidation and that the oxidation of the material occurs over multiple individual events.

For the 50 nm AgNPs the mean charges passed per spike were comparable at all times throughout the chronoamperograms, and showed no noticeable variation with immersion time; this data is presented in the SI section S4. Considering this observation and the similarity of the nano-impact frequency to that predicted by a steady-state flux above, this preliminary result is consistent with the complete oxidation of 50 nm AgNPs, which will be further explored in the next section. For the 100 nm AgNPs however, as presented in the SI section S5, whilst the mean charges passed per spike at short t and long t are comparable for short immersion times, they differ markedly for longer immersion times (at most a factor of 5 larger for an immersion time of 120 s). This further supports the notion that the initial spike features present in the current-time trace are a result of multiple partial oxidations of AgNPs pre-adsorbed onto the electrode.

When running cyclic voltammetry on such AgNPs solutions, the slow increasing potential steps result in the pre-adsorbed material on the electrode surface being oxidised and appearing as one distinct stripping wave [32], occurring at ca. 0.14 V (vs. SCE). The slow oxidation of this material on the surface precludes the complicating factors described above,

particularly considering that the nano-impact charges recorded at 0.2 – 0.4 V are neglected in the subsequent charge analysis. As a result, cyclic voltammetry, for this study, is not compromised by the variations of electrode immersion time prior to chronoamperogram commencement for analysis of 100 nm AgNPs. Consequently, the following electrochemical studies will employ cyclic voltammetry to further investigate the partial or complete oxidation of 50 nm or 100 nm AgNPs using a variable temperature study.

Variable Temperature Nano-Impacts Study

Further nano-impacts of AgNPs were investigated at different temperatures through the use of cyclic voltammetry. Measurements were carried out by initially scanning anodically in the potential range 0 to 0.8 V (vs. SCE) in 1.5 pM 100 nm AgNP suspensions containing 20 mM KCl at a carbon microdisc (33 μ m diameter) working electrode. Figure 4 presents representative cyclic voltammograms at 15°C, 25°C, 35°C and 50°C respectively.

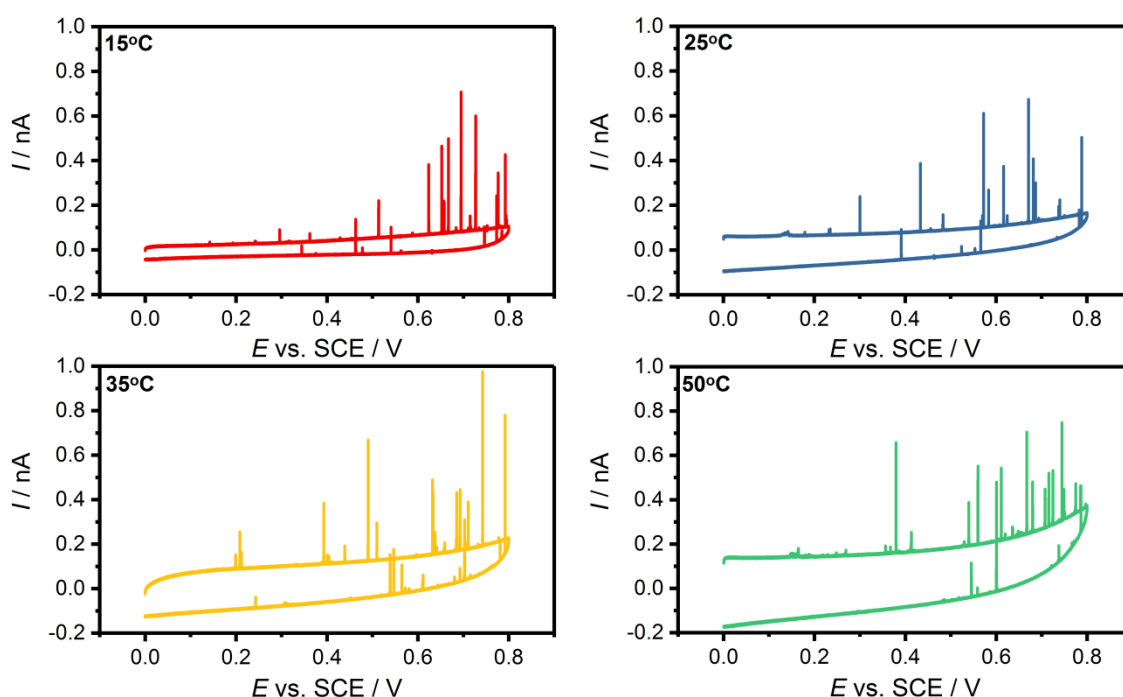


Figure 4. Representative examples of cyclic voltammograms run in suspensions of 1.5 pM 100 nm AgNPs in 20 mM KCl at a carbon microdisc electrode at four different temperatures at a scan rate of 10 mV s⁻¹.

Integration of the current under each spike with respect to time gives the amount of charge transferred in a single nanoparticle oxidation event. The charges of the spikes on the forward scans were analysed as a function of potential at each temperature. The average charge passed per individual spike event was found to be dependent on potential; at lower potentials (0.2 to 0.4 V vs. SCE), the calculated charge was on average smaller than for higher potentials

(0.4 to 0.8 V vs. SCE), as presented in Figure 5 a). This threshold in charge magnitude can be ascribed to the slow kinetics of the AgNP oxidation process at low overpotentials [36]. It should be noted that the charge at these lower potentials may be underestimated due to a poorer signal-to-noise ratio resulting in slower and lower current processes being obscured in the background noise as reported previously [22].

In the lower potential range, noting the sizeable mean standard error, there is a small decrease in observed charge per impact event with temperature. At higher potentials the charge passed per impact spike goes through a maximum at 25°C, before falling at 35°C and 50°C. This can be rationalised by considering that at higher temperatures, the nanoparticles have a higher energy, and hence there is an increased probability of them leaving the electrode surface more quickly, with a lesser percentage of oxidation completed prior to departure. However, at low temperatures, the decrease in charge at 15°C likely reflects the contribution of slow oxidation kinetics. At lower potentials, the addition of the slower kinetics of the process due to the low applied potential to the above factor results in a continuous decrease of mean charge passed per impact with temperature. It should be noted that the mean charges passed per spike feature are comparable in both potential ranges at 15°C. The slow kinetics of the oxidation reaction at this lower temperature may reflect the contribution of other factors such as the exchange or 'gating' of the nanoparticle capping agent prior to electron transfer [37]. Given the threshold above 0.4 V, the data for the potential range 0.4-0.8 V will be considered for the subsequent charge analysis.

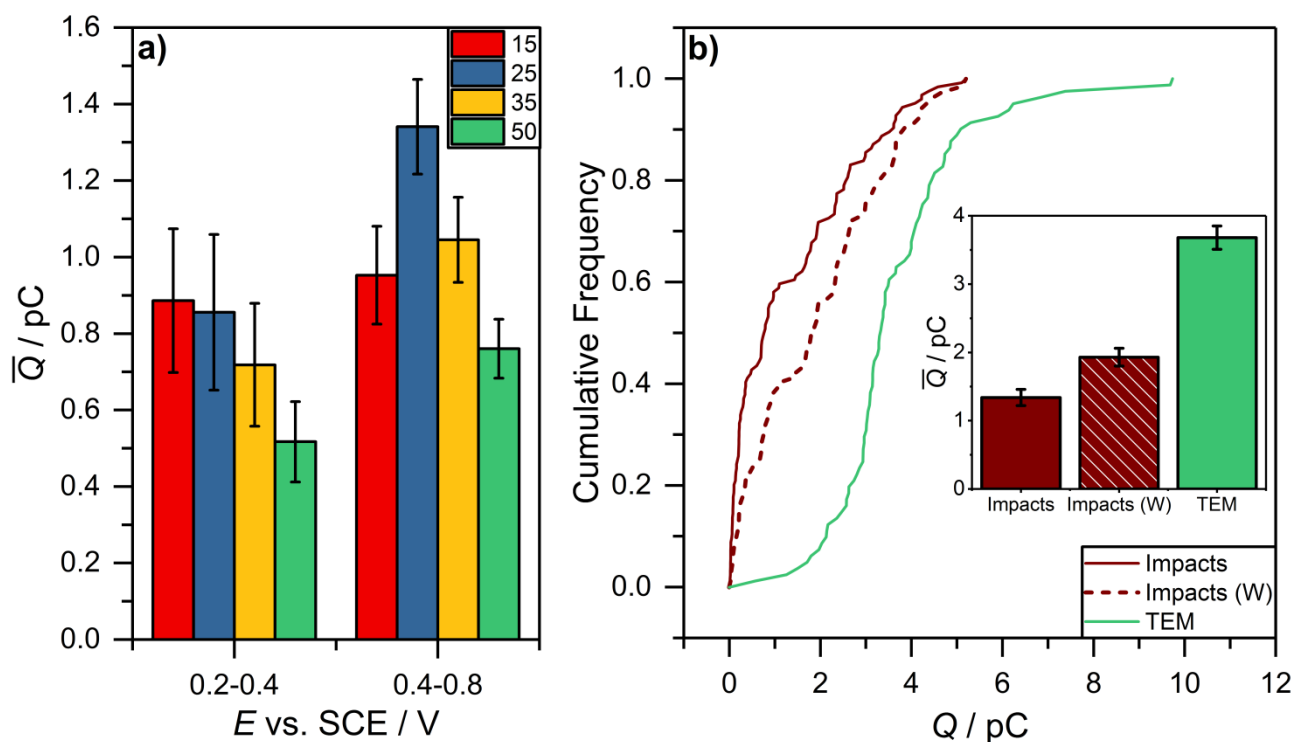


Figure 5. a) Mean charge passed per spike and associated standard error for impacts of 100 nm AgNPs in the potential ranges 0.2 – 0.4 V and 0.4 – 0.8 V at four temperatures. b) Cumulative frequency charge distributions at 25°C for nano-impact spike charges in the range 0.4-0.8 V with and without applying a diffusional weighting (dotted and solid brown lines respectively). Green solid line shows obtained charge distribution from TEM images. Inlay depicts the mean charge passed per spike and associated mean standard error for the three methods.

Comparison of charge data obtained from the nano-impact experiments with the results from TEM imaging demands several considerations to be made. First, the sizing *via* the electrochemical nano-impact technique is inherently biased towards the detection of smaller nanoparticles due to their higher diffusion coefficients. Each nano-impact gives a measure of the NP volume and hence, assuming a spherical NP, the volume gives a direct measure of the diffusion coefficient. Furthermore, assuming a steady-state flux to the electrode, the probability of observing a NP is proportional to its diffusion coefficient. These acknowledgments allow the electrochemically determined charge distribution to be corrected by weighting each nanoparticle impact with a factor of $Q^{1/3}$, where Q is the charge passed during a single impact event. This weighting originates from the Stokes-Einstein equation:

$$(3) \quad D = \frac{k_B T}{6\pi\eta r_{NP}}$$

where D is the diffusion coefficient of the nanoparticle, T is the temperature, η is the viscosity of the solvent and r_{NP} is the radius of the nanoparticle. The assumption that the nanoparticles are spherical gives $V \propto r^3$, leading to $D \propto 1/V^{1/3}$.

The mean charge passed per impact at 25°C in Figure 5 a) of 1.34 ± 0.12 pC becomes 1.93 ± 0.13 pC when diffusional weighting is taken into account; notably this is still significantly less than the 3.68 ± 0.17 pC predicted from TEM imaging, as presented in Figure 6 b). Even when statistically clustering spikes together on the basis of a window of time where there is a 99% probability of maximally one event occurring (see SI section S6) *and* applying a diffusional weighting, the mean charge passed per impact only rises to 2.88 ± 0.21 pC, *ca.* 22% lower than the estimated charge from TEM imaging. To restate this point, even when windowing and weighting the data it is not possible to get a good agreement (within known experimental error) between the electrochemical and microscopy sizing data for the 100 nm particles; indicating that for these particles, under the present experimental conditions, the individual nano-oxidation events do not go to completion. Moreover, windowing the data in this way still results in a higher impact frequency than that predicted by a steady-state flux; this is presented in the SI section S6 c). The discrepancies in the size distributions presented in Figure 6 b) result from the presence of a large number of lower charge magnitude impacts; the data presented here is highly indicative of single nanoparticles undergoing multiple oxidations at the electrode. These oxidations do not go to completion, with a significant probability that the partially oxidised nanoparticle diffuses away from the electrode prior to complete oxidation.

For comparison, an analogous variable temperature study was carried out on suspensions of the smaller 50 nm AgNPs at the carbon microdisc electrode; the results are presented in the SI section S7. Previous work has shown that the magnitude of the charges passed per nano-impact for oxidation of 50 nm AgNPs is independent of temperature at a gold microdisc electrode [21]. For the studies at 15°C and 25°C, a similar threshold potential was found above which the magnitude of the charge passed per impact was larger (see SI Figure S7 a)), hence the potential range 0.5 to 0.8 V was chosen for the subsequent charge analysis. The reason for this threshold is likely the same as that described above for the 100 nm AgNPs. The charge distributions (SI Figure S7 b)) for the studies at 15°C and 25°C are extremely comparable; the mean charges are 0.195 ± 0.008 pC and 0.201 ± 0.01 pC respectively. This lack of sensitivity to temperature is consistent with complete oxidation of these 50 nm AgNPs. However, the charge distribution and associated mean charge observed at 50°C is slightly higher with a

value of 0.247 ± 0.009 pC. There are several possible interpretations of this increase in value. First, the measured noise of the system increases with temperature, and as such some of the smaller current magnitude spikes may be lost in this noise [22]. Second, an increase in frequency at this higher temperature may result in the overlapping of spikes in the current-time trace, resulting in an overestimation of the charge. In either case in analogy with the results presented for the data measured for 100 nm particles, if the oxidation was not being driven to completion one would expect a corresponding decrease and not an increase in the charge passed per event at high temperatures.

By taking into account the diffusional weighting described above, the mean charge per impact for the 50 nm AgNPs at 25°C rises to $0.248 \text{ pC} \pm 0.011 \text{ pC}$. This is in reasonable agreement with the value estimated from the TEM images of $0.281 \pm 0.025 \text{ pC}$; the charge distributions are comparable and are presented in the SI Figure S7 c). The standard deviations of the weighted electrochemically determined distribution and the distribution from TEM are fairly high; 0.185 and 0.167 pC respectively, reflecting the heterogeneity in the nanoparticle sample. The insensitivity of the mean charge observed at lower temperatures, the corroboration with TEM and the similarity of the impact frequency to that predicted by a steady-state flux (Figure 3 a)) are consistent with the complete oxidation of this size of nanoparticles, in contrast to the 100 nm AgNPs studied above.

Conclusions

The use of a variable temperature study has been employed to differentiate between the extents of oxidation of two sizes of silver nanoparticles. The variation in the charge passed per nano-impact event at differing potentials has been accounted for in accordance with the literature. It has been shown that for larger sized nanoparticles, single nanoparticles undergo multiple oxidations at the electrode, and that these oxidations do not go to completion. This has been evidenced by the dependency of the nanoparticle-electrode impact frequency on the time the electrode is exposed to the nanoparticle suspension prior to the start of the chronoamperogram; the decrease in charge passed per nano-event at high temperatures, stemming from an increased probability of nanoparticle departure from the electrode prior to complete oxidation; and comparison of expected and observed frequencies of nano-impacts. Even when accounting for factors that result in an underestimation of the charge passed, the obtained values for the 100 nm particles are dramatically (*ca.* 48%) lower than the estimated charge values obtained from TEM imaging assuming complete oxidation. Conversely, the relative insensitivity of the charge passed per nano-impact event and the comparable expected and observed nano-impact frequency for the smaller sized nanoparticles is consistent with their complete oxidation, in one single event. As such, a variable temperature study has facilitated the differentiation between the oxidation processes occurring for the two sizes of nanoparticles.

Acknowledgements

The research is sponsored by the funding from the European Research Council under the European Union Seventh Framework Programme (FP/2007-2013)/ERC Grant Agreement No. [320403].

References

- [1] S. Eloul, R.G. Compton, General Model of Hindered Diffusion, *J. Phys. Chem. Lett.* 7 (2016) 4317–4321. doi:10.1021/acs.jpcllett.6b02275.
- [2] S. Eloul, E. Kätelhön, R.G. Compton, When does near-wall hindered diffusion influence mass transport towards targets?, *Phys. Chem. Chem. Phys.* 18 (2016) 26539–26549. doi:10.1039/C6CP05716K.
- [3] I.K. Snook, W. van Megen, Solvation forces in simple dense fluids. I, *J. Chem. Phys.* 72

- (1980) 2907–2913. doi:10.1063/1.439489.
- [4] J.N. Israelachvili, Intermolecular and surface forces, Academic Press, 2011.
 - [5] H. Krupp, Particle adhesion theory and experiment, *Adv. Colloid Interface Sci.* 1 (1967) 111–239. doi:10.1016/0001-8686(67)80004-6.
 - [6] X. Wu, E. Sacher, M. Meunier, The effects of hydrogen bonds on the adhesion of inorganic oxide particles on hydrophilic silicon surfaces, *J. Appl. Phys.* 86 (1999) 1744. doi:10.1063/1.370956.
 - [7] R.A. Bowling, An Analysis of Particle Adhesion on Semiconductor Surfaces, *J. Electrochem. Soc.* 132 (1985) 2208–2214. doi:10.1149/1.2114320.
 - [8] M. Polin, D.G. Grier, Y. Han, Colloidal electrostatic interactions near a conducting surface, *Phys. Rev. E* 76 (2007) 041406. doi:10.1103/PhysRevE.76.041406.
 - [9] P.H. Robbs, N. V. Rees, Nanoparticle electrochemistry, *Phys. Chem. Chem. Phys.* 18 (2016) 24812–24819. doi:10.1039/C6CP05101D.
 - [10] S. V. Sokolov, S. Eloul, E. Kätelhön, C. Batchelor-McAuley, R.G. Compton, Electrode–particle impacts: a users guide, *Phys. Chem. Chem. Phys.* 19 (2017) 28–43. doi:10.1039/C6CP07788A.
 - [11] J.G. Simmons, Generalized Formula for the Electric Tunnel Effect between Similar Electrodes Separated by a Thin Insulating Film, *J. Appl. Phys.* 34 (1963) 1793–1803. doi:10.1063/1.1702682.
 - [12] Y. V Sharvin, A Possible Method for Studying Fermi Surfaces, *Sov. Phys. JETP* 21 (1965) 655. <http://www.jetp.ac.ru/cgi-bin/e/index/e/21/3/p655?a=list> (accessed May 2, 2018).
 - [13] P.P. Edwards, H.B. Gray, M.T.J. Lodge, R.J.P. Williams, Electron Transfer and Electronic Conduction through an Intervening Medium, *Angew. Chemie Int. Ed.* 47 (2008) 6758–6765. doi:10.1002/anie.200703177.
 - [14] Y.-G. Zhou, N. V. Rees, R.G. Compton, The Electrochemical Detection and Characterization of Silver Nanoparticles in Aqueous Solution, *Angew. Chemie Int. Ed.* 50 (2011) 4219–4221. doi:10.1002/anie.201100885.
 - [15] E. Kätelhön, E.E.L. Tanner, C. Batchelor-McAuley, R.G. Compton, Destructive nano-impacts: What information can be extracted from spike shapes?, *Electrochim. Acta* 199 (2016) 297–304. doi:10.1016/J.ELECTACTA.2016.02.031.
 - [16] T.R. Bartlett, S. V. Sokolov, R.G. Compton, Electrochemical Nanoparticle Sizing Via Nano-Impacts: How Large a Nanoparticle Can be Measured?, *ChemistryOpen* 4 (2015) 600–605. doi:10.1002/open.201500061.

- [17] E.J.F. Dickinson, N. V. Rees, R.G. Compton, Nanoparticle–electrode collision studies: Brownian motion and the timescale of nanoparticle oxidation, *Chem. Phys. Lett.* 528 (2012) 44–48. doi:10.1016/J.CPLETT.2012.01.036.
- [18] J. Ustarroz, M. Kang, E. Bullions, P. Unwin, Impact and oxidation of single silver nanoparticles at electrode surfaces: one shot versus multiple events, *Chem. Sci.* 8 (2017) 1841–1853. doi:10.1039/C6SC04483B.
- [19] S.M. Oja, D.A. Robinson, N.J. Vitti, M.A. Edwards, Y. Liu, H.S. White, B. Zhang, Observation of Multipeak Collision Behavior During the Electro-Oxidation of Single Ag Nanoparticles, *J. Am. Chem. Soc.* 139 (2017) 708–718. doi:10.1021/jacs.6b11143.
- [20] K.J. Krause, F. Brings, J. Schnitker, E. Kätelhön, P. Rinklin, D. Mayer, R.G. Compton, S.G. Lemay, A. Offenhäusser, B. Wolfrum, The Influence of Supporting Ions on the Electrochemical Detection of Individual Silver Nanoparticles: Understanding the Shape and Frequency of Current Transients in Nano-impacts, *Chem. - A Eur. J.* 23 (2017) 4638–4643. doi:10.1002/chem.201605924.
- [21] X. Li, C. Batchelor-McAuley, J.K. Novev, R.G. Compton, A thermostated cell for electrochemistry: minimising natural convection and investigating the role of evaporation and radiation, *Phys. Chem. Chem. Phys.* 20 (2018) 11794–11804. doi:10.1039/C8CP01360H.
- [22] C.A. Little, R. Xie, C. Batchelor-McAuley, E. Katelhon, X. Li, N.P. Young, R.G. Compton, A Quantitative Methodology for the Study of Particle-Electrode Impacts, *Phys. Chem. Chem. Phys.* 20 (2018) 13537–13546. doi:10.1039/C8CP01561A.
- [23] C. Batchelor-McAuley, J. Ellison, K. Tschulik, P.L. Hurst, R. Boldt, R.G. Compton, In situ nanoparticle sizing with zeptomole sensitivity, *Analyst.* 140 (2015) 5048–5054. doi:10.1039/C5AN00474H.
- [24] J. Novev, R.G. Compton, Natural convection effects in electrochemical systems, *Curr. Opin. Electrochem.* 7 (2018) 118–129. doi: 10.1016/j.coelec.2017.09.010
- [25] T. Ung, M. Giersig, D. Dunstan, P. Mulvaney, Spectroelectrochemistry of Colloidal Silver, *Langmuir.* 13 (1997) 1773–1782. doi:10.1021/LA960863Z.
- [26] L. Kelly, E. Coronado, L.L. Zhao, G.C. Schatz, The Optical Properties of Metal Nanoparticles: The Influence of Size, Shape, and Dielectric Environment, *J. Phys. Chem. B.* 107 (2003) 668–677. doi:10.1021/JP026731Y.
- [27] N.G. Bastús, J. Piella, V. Puentes, Quantifying the Sensitivity of Multipolar (Dipolar, Quadrupolar, and Octapolar) Surface Plasmon Resonances in Silver Nanoparticles: The Effect of Size, Composition, and Surface Coating, *Langmuir.* 32 (2016) 290–300.

doi:10.1021/acs.langmuir.5b03859.

- [28] Derjaguin, L. Landau, Theory of the Stability of Strongly Charged Lyophobic Sols and of the Adhesion of Strongly Charged Particles in Solutions of Electrolytes, *Acta Phys. Chim. URSS.* 14 (1941) 633–62.
- [29] E.J.W. Verwey, J.T.G. Overbeek, *Theory of the Stability of Lyophobic Colloids*, Elsevier: Amsterdam, 1948.
- [30] D.K. Bhui, H. Bar, P. Sarkar, G.P. Sahoo, S.P. De, A. Misra, Synthesis and UV–vis spectroscopic study of silver nanoparticles in aqueous SDS solution, *J. Mol. Liq.* 145 (2009) 33–37. doi:10.1016/J.MOLLIQ.2008.11.014.
- [31] S.V. Sokolov, K. Tschulik, C. Batchelor-McAuley, K. Jurkschat, R.G. Compton, Reversible or Not? Distinguishing Agglomeration and Aggregation at the Nanoscale, *Anal. Chem.* 87 (2015) 10033–10039. doi:10.1021/acs.analchem.5b02639.
- [32] K. Ngamchuea, R.O.D. Clark, S. V. Sokolov, N.P. Young, C. Batchelor-McAuley, R.G. Compton, Single Oxidative Collision Events of Silver Nanoparticles: Understanding the Rate-Determining Chemistry, *Chem. - A Eur. J.* 23 (2017) 16085–16096. doi:10.1002/chem.201703591.
- [33] Y. Saito, A Theoretical Study on the Diffusion Current at the Stationary Electrodes of Circular and Narrow Band Types, *Rev. Polarogr.* 15 (1968) 177–187. doi:10.5189/revpolarography.15.177.
- [34] C.A. Little, C. Batchelor-McAuley, K. Ngamchuea, C. Lin, N.P. Young, R.G. Compton, Coupled Optical and Electrochemical Probing of Silver Nanoparticle Destruction in a Reaction Layer, *ChemistryOpen.* (2018) In Press. doi:10.1002/open.201800048.
- [35] K.J. Krause, A. Yakushenko, B. Wolfrum, Stochastic On-Chip Detection of Subpicomolar Concentrations of Silver Nanoparticles, *Anal. Chem.* 87 (2015) 7321–7325. doi:10.1021/acs.analchem.5b01478.
- [36] E.N. Saw, M. Kratz, K. Tschulik, Time-resolved impact electrochemistry for quantitative measurement of single-nanoparticle reaction kinetics, *Nano Res.* 10 (2017) 3680–3689. doi:10.1007/s12274-017-1578-3.
- [37] E.E.L. Tanner, K. Tschulik, R. Tahany, K. Jurkschat, C. Batchelor-McAuley, R.G. Compton, Nanoparticle Capping Agent Dynamics and Electron Transfer: Polymer-Gated Oxidation of Silver Nanoparticles, *J. Phys. Chem. C.* 119 (2015) 18808–18815. doi: 10.1021/acs.jpcc.5b05789